RSC Advances

PAPER

View Article Online
View Journal | View Issue

Cite this: *RSC Adv.*, 2018, **8**, 14422

Structural elucidation of NASICON ($Na_3Al_2P_3O_{12}$) based glass electrolyte materials: effective influence of boron and gallium†

Amarnath R. Allu, ‡*[a] Sathravada Balaji, ‡[a] Kavya Illath,[b] Chaithanya Hareendran,[b] T. G. Ajithkumar,[b] Kaushik Biswas[a] and K. Annapurna*[a]

Understanding the conductivity variations induced by compositional changes in sodium super ionic conducting (NASICON) glass materials is highly relevant for applications such as solid electrolytes for sodium (Na) ion batteries. In the research reported in this paper, NASICON-based NCAP glass ($Na_{2.8}Ca_{0.1}Al_2P_3O_{12}$) was selected as the parent glass. The present study demonstrates the changes in the Na^+ ion conductivity of NCAP bulk glass with the substitution of boron (NCABP: $Na_{2.8}Ca_{0.1}Al_2B_{0.5}P_{2.7}O_{12}$) and gallium (NCAGP: $Na_{2.8}Ca_{0.1}Al_2Ga_{0.5}P_{2.7}O_{12}$) for phosphorus and the resulting structural variations found in the glass network. For a detailed structural analysis of NCAP, NCABP and NCAGP glasses, micro-Raman and magic angle spinning-nuclear magnetic resonance (MAS-NMR) spectroscopic techniques (for ^{31}P, ^{27}Al, ^{23}Na, ^{11}B and ^{71}Ga nuclei) were used. The Raman spectrum revealed that the NCAP glass structure is more analogous to the $AlPO_4$ mesoporous glass structure. The ^{31}P MAS-NMR spectrum illustrated that the NCAP glass structure consists of a high concentration of Q^0 (3Al) units, followed by Q^0 (2Al) units. The ^{27}Al MAS-NMR spectrum indicates that alumina exists at five different sites, which include AlO_4 units surrounded by AlO_6 units, $Al(OP)_4$, $Al(OP)_5$, $Al(OAl)_6$ and $Al(OP)_6$, in the NCAP glass structure. The ^{31}P, ^{27}Al and ^{11}B MAS-NMR spectra of the NCABP glass revealed the absence of B–O–Al linkages and the presence of B_3–O–B_4–O–P_4 linkages which further leads to the formation of borate and borophosphate domains. The ^{71}Ga MAS-NMR spectrum suggests that gallium cations in the NCAGP glass compete with the alumina cations and occupy four (GaO_4), five (GaO_5) and six (GaO_6) coordinated sites. The Raman spectrum of NCAGP glass indicates that sodium cations have also been substituted by gallium cations in the NCAP glass structure. From impedance analysis, the dc conductivity of the NCAP glass ($\sim 3.13 \times 10^{-8}$ S cm^{-1}) is slightly decreased with the substitution of gallium ($\sim 2.27 \times 10^{-8}$ S cm^{-1}) but considerably decreased with the substitution of boron ($\sim 1.46 \times 10^{-8}$ S cm^{-1}). The variation in the conductivity values are described based on the structural changes of NCAP glass with the substitution of gallium and boron.

Received 26th February 2018
Accepted 4th April 2018

DOI: 10.1039/c8ra01676c

rsc.li/rsc-advances

1. Introduction

The existing technologies used today for electrochemical devices such as batteries are a better alternative to the dwindling fossil fuels in providing energy.[1,2] This is relevant, because commercialized lithium ion batteries (LIBs) technology from 1991 is widely used for portable electronic devices.[3] Nevertheless, there are increasing needs to replace the existing LIBs because of the increasing cost of production of LIBs and because lithium is scarce.[1,4,5] In searching for alternative energy sources, abundant, economical and non-toxic sodium (Na) metal has been considered by the scientific community and continuous efforts have been carried out so far for the development of Na-batteries.[5–8] Although the concept of Na-batteries has been proposed and proved several years ago, the topic has rematerialized again. Because of the heavier weight of Na batteries, they exhibit a primary disadvantage of having a low theoretical energy density compared to their lithium counterparts. Recent studies proposed that the output voltage of certain Na-based materials could compete with that of lithium batteries and thus, opened the opportunity to investigate and develop the Na-based materials.[5–8] Considerable efforts are presently in progress to improve appropriate electrolyte and electrode materials for practically feasible Na-batteries.[7,9,10] Among the various types of electrolyte materials, solid electrolyte materials

[a]*Glass Division, CSIR-Central Glass and Ceramic Research Institute, 700032, Kolkata, India. E-mail: aareddy@cgcri.res.in; annapurnak@cgcri.res.in; Fax: +91-33-24730957; Tel: +91-33-23223421*

[b]*Central NMR Facility and Physical and Materials Chemistry Division, CSIR-National Chemical Laboratory, 411008, Pune, India*

† Electronic supplementary information (ESI) available: ^{27}Al 3Q MAS-NMR and deconvolution of ^{27}Al MAS-NMR spectra. Impedance analysis and fitted data for the equivalent circuit. See DOI: 10.1039/c8ra01676c

‡ These authors contributed equally.

have attracted significant interest compared to those of the liquid electrolytes because of the protection from leakage, volatilization, or flammability.[10–12] However, to create the solid electrolyte batteries, a high ionic conductivity of electrolyte materials ($\sigma_{Na} \gtrsim 10^{-4}$ S cm^{-1}) at room temperature (RT) is required.

Many studies have already been carried out to develop a suitable RT solid electrolyte material.[13–16] In this regard non-oxide chalcogenide glasses ($Na_2(Ga_{0.1}Ge_{0.9})_2Se_{4.95}$ and Na_2S–SiS_2)[15,17] and oxide-based phosphate glasses (P_2O_5–FeO–Na_2O and P_2O_5–B_2O_3–Na_2O)[16,18] are important. Although the non-oxide based electrolyte materials are superior compared to oxide materials, the high cost and poor ambient stability limit their practical implementation.[15,16] However, sodium super ionic conductor (NASICON) based phosphate glass and glass-ceramics are better suited as the RT electrolyte materials with Na^+ ions as the mobile species.[14,19–21] The maximum value of conductivity has been obtained for the $Na_{3.1}Zr_{1.95}Mg_{0.05}Si_2PO_{12}$ which exhibits a high RT ionic conductivity of 3.5×10^{-3} S cm^{-1}.[14] In general, NASICON and the relevant solid electrolytes are produced using a conventional solid state reaction process, which includes sintering and calcination over 1100 °C.[22] The sintering process usually leads to the formation of voids and may disturb the development of new structured materials to gain high conductivity.

Glass-based electrolyte materials have numerous advantages because of their isotropic properties for ion migration. These advantages are: glasses are easy to mould, having low cost and desired properties can be easily tailored by changing their chemical compositions.[23] More importantly, the formation of voids during the sintering and calcination process can be easily avoided if the designed glass composition melts at a low temperature. It is also interesting to note that glasses having higher ionic conductivities than crystalline materials of the same compositions are fairly common. For example, the conductivity of glassy $Li_{3.6}P_{0.4}Si_{0.6}O_4$ at 25 °C is ten times higher than that of its polycrystalline form.[24] Moreno-Real *et al.* have studied the structure and conductivity of glass and crystalline $Na_3Al_2P_3O_{12}$ material.[19] It was also observed that the conductivity of glass (v-$Na_3Al_2P_3O_{12}$) material is higher than the conductivity of crystalline (c-$Na_3Al_2P_3O_{12}$) material. It was also found that v-$Na_3Al_2(PO_4)_3$ has no significant grain boundary contributions to the resistance. These examples clearly illustrate the possibility for the development of highly conducting glass-based materials rather than the crystalline materials. However, so far, only a few reports were found highlighting the sodium ionic conductors with the NASICON-type structure containing Al cations.[19,25,26] Therefore, the present research reported here, aims at developing the Al-containing NASICON ($Na_3Al_2P_3O_{12}$) glass for use as a solid electrolyte material by understanding the glass structure and the modifications that occur in the structure with the changes in its chemical composition.

To achieve and to optimise the desired properties from the glass-based materials, it is helpful to have a clear picture of the structure and the role of each cation.[27] It is known that to achieve greater conductivity ($\sigma = c\mu q$), in addition to increasing the concentration (c) and mobility (μ) of the charge carriers, understanding the "structure" also plays a crucial role, and it should be considered as one of the key factors in designing the glass-based electrolyte material.[28,29] Very recently, glass and glass-ceramic bilayer sealants for solid oxide fuel cell applications have been developed by systematically varying the chemical composition of glasses through an understanding of the structure of glasses.[23] Among the various techniques, magic angle spinning-nuclear magnetic resonance (MAS-NMR) and micro-Raman confocal spectroscopies are reliable techniques for structural characterization of glass materials. Solid-state NMR is particularly applicable for probing the coordination numbers of spin active nuclei such as ^{23}Na, ^{31}P and ^{27}Al, network connectivity and, in favourable cases, next-nearest neighbour (NNN) connectivity, whilst Raman and infrared spectroscopy can be utilised to probe the nature of the bond between the metal cation and its surrounding oxygen anion.[30,31]

In the present study, the NASICON-based glasses with a modified chemical formula of $Na_{2.8}Ca_{0.1}Al_2P_3O_{12}$ (NCAP) was considered as a starting glass composition to design and develop the solid-based electrolyte material. The structure of the NCAP glass was studied thoroughly. The NCAP glass composition was further modified using the substitution of boron (B) and gallium (Ga) for phosphorus (P) according to the chemical formula of $Na_{2.8}Ca_{0.1}Al_2P_{2.7}X_{0.5}O_{12}$ (where X = B and Ga). The B and Ga cations were substituted to observe the changes in the structure of the NCAP glass and thereby to utilise them for further improvement in the conductivity of NCAP glass. The ^{27}Al, ^{11}B, ^{71}Ga, ^{23}Na, and ^{31}P MAS-NMR and micro-Raman techniques were utilised to elucidate the structure of the newly designed glasses. The modified glass materials were also characterised, using impedance measurements, to check their applicability as an electrolyte material for batteries.

2. Experimental

The experimental glasses in bulk form were prepared using the melt quenching technique. High purity powders of ammonium dihydrogen phosphate [$(NH_4)H_2PO_4$], sodium carbonate (Na_2CO_3), calcium carbonate ($CaCO_3$), aluminium oxide (Al_2O_3), boric acid (H_3BO_3) and gallium oxide (Ga_2O_3) were used to prepare the newly designed glasses. Homogeneous mixtures of batches obtained by hand grinding appropriate quantities of ingredients in agate mortar for about 45 min, were preheated in an alumina crucible for decarbonisation using the following heat treatment schedule: (i) RT to 350 °C at a heating rate (β) of 1 °C min^{-1} followed by a dwell time of 6 h at 350 °C; (ii) from 350 °C to 600 °C at $\beta = 1$ °C min^{-1} followed by a dwell time of 3 h at 600 °C; and (iii) from 600 °C to 900 °C at $\beta = 4$ °C min^{-1} followed by a dwell time of 1 h at 900 °C. The decarbonized batch mixture was first melted in an alumina crucible and then re-melted again in a platinum crucible to obtain better homogeneity at 1350 °C for 2 h, in an air atmosphere. The glasses in bulk form were obtained by quenching the glass melt into a pre-heated (400 °C) stainless steel mould followed by annealing at temperatures around the glass transition temperature of 350 °C.[19] The amorphous nature of the glasses was confirmed

using X-ray diffraction (XRD) analysis. The new glass compositions were labelled based on the chemical formula obtained after the substitution of X^{3+} cations (X = B and Ga) for P^{5+} cations: $Na_{2.8}Ca_{0.1}Al_2B_{0.5}P_{2.7}O_{12}$ (NCABP) for X = B and $Na_{2.8}Ca_{0.1}Al_2Ga_{0.5}P_{2.7}O_{12}$ (NCAGP) for X = Ga. The detailed chemical compositions (in mol%) of the glasses are provided in Table 1.

Raman spectra for bulk glass samples were obtained using a Horiba LabRam HR 800 Evolution confocal Raman microscope, with a 488 nm argon ion excitation laser source (10 mW) focused with an 100× objective lens (numerical aperture = 0.9) with a spot size of ~3.14 μm^2. The Raman radiation collected was dispersed with a 600 lines mm^{-1} grating and focused on a Peltier-cooled charge-coupled device (CCD) detector which allowed a spectral resolution of approximately 2 cm^{-1}. All the spectra were recorded in the range of 200 to 1500 cm^{-1} with an integration time of 10 s and 20 accumulations per spectrum.

All the solid-state NMR experiments were carried out on a Bruker Avance HD 700 MHz spectrometer equipped with a superconducting magnet of 16.5 T. The single pulse ^{23}Na, ^{27}Al, ^{31}P MAS-NMR measurements were carried out in a 2.5 mm Bruker TriGamma probe with Larmor frequency of 185.198 MHz for ^{23}Na, 182.432 MHz for ^{27}Al and 283.418 MHz for ^{31}P. The samples were packed in 2.5 mm zirconia rotors and were spun at 32 kHz. The relaxation delay for ^{31}P, ^{23}Na and ^{27}Al were 1100 s, 1 s and 3 s, respectively, and the number of transients were 16, 256 and 2048, respectively. The ^{27}Al 3-quantum magic-angle spinning NMR (3Q MAS-NMR) spectra were acquired using a Bruker 1.3 mm MAS probe which was packed in a 1.3 mm rotor and spun at 32 kHz. The $64t_1$ points with 600 transients per t_1 point were acquired with a 1 s recycling time. A very high radio frequency power of 200 kHz was used for this experiment. The ^{11}B and ^{71}Ga experiments were acquired using a Hahn echo pulse sequence in a Bruker 1.3 mm MAS probe at a spinning frequency of 60 kHz at Larmor frequencies of 224.5 MHz and 213.477 MHz, respectively. The chemical shifts of ^{31}P, ^{23}Na, ^{27}Al, ^{11}B and ^{71}Ga were compared to 85% of aqueous phosphoric acid, 1 M NaCl solution, 1 M aluminum nitrate solution, 1 M boric acid solution (19.5 ppm), and 1 M gallium nitrate solution, respectively. To extract the NMR parameters, chemical shift, quadrupolar coupling constant and integrated peak area of the individual peaks from the experimental spectra, the DMFIT programme developed by Massiot was used.[32]

For impedance analysis, all the glass samples were uniformly cut into to 8 × 8 mm^2 squares with a thickness of 1.5 mm and polished to optical grade quality and then hand coated with high conductivity (volume resistivity = 0.0174 ohm cm) silver epoxy (Cat. no. 8331-14G, MG Chemicals Ltd., Canada). The silver coated glass samples were cured over night at ~100 °C in an air circulating oven. The conductivity measurements were carried out in the frequency range of 50 Hz to 1 MHz with 3 V root mean square (rms) using an LCR Hi-Tester model HIOKI-3532-50 (Hioki E. E. Corporation, Japan). A two-probe setup with test leads connected to a Test Fixture HIOKI-9262 was used to acquire the data. The real time data was acquired using HIOKI LCR HiTESTER software version 4.03E. The temperature dependent frequency characteristics of the glass samples were measured from RT to 200 °C with a 25 °C interval using a DPI-1200 high temperature dry calibrator (Divya Process Instruments) with temperature accuracy of ±1 °C.

Table 1 Chemical composition of glasses (mol%). (Al_2O_3: aluminium oxide, B_2O_3: boron trioxide, CaO: calcium oxide, Ga_2O_3: gallium oxide, Na_2O: sodium oxide, P_2O_5: phosphorus pentoxide)

	NCAP	NCABP	NCAGP
Na_2O	35.0	34.1	34.1
CaO	02.5	02.4	02.5
Al_2O_3	25.0	24.4	24.3
P_2O_5	37.5	33.0	33.0
B_2O_3	—	06.1	—
Ga_2O_3	—	—	06.1

3. Results

3.1 Raman spectroscopy

Fig. 1 displays the Raman spectra of all the glasses. The vibrational bands in the Raman spectra for all the glasses were observed in the following three regions: (i) low frequency region (200–650 cm^{-1}), intermediate frequency region (650–850 cm^{-1}), and high frequency regions (850–1400 cm^{-1}). The low frequency region is dominated by five easily identified medium intensity peaks at around 310, 460, 500, 575 and 620 cm^{-1}. The intermediate frequency region contains only one low intensity broad peak at ~730 cm^{-1}, and the high frequency region is dominated by two high intensity peaks at ~1042 and ~1210 cm^{-1}.

The Raman spectrum for observed NCAP glass was similar to that of $Na_3Al_2P_3O_{12}$ (NAP) glass reported by Yifen *et al.*[33] Therefore, the peak obtained at 1040 cm^{-1} can be unambiguously assigned to the symmetric stretching vibrations of the $AlPO_4$ groups, in which the phosphorus tetrahedral units are surrounded by alumina tetrahedral units as the second nearest neighbour. Nevertheless, a slight discrepancy was found when assigning the peak observed at 1210 cm^{-1} because of the flat and broad nature of the peak. In order to assign the peak to specific structural units, the deconvolution procedure was used

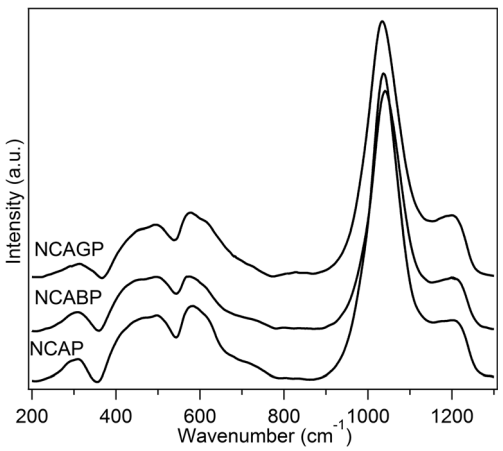

Fig. 1 Micro-Raman spectra for NCAP, NCABP and NCAGP glasses.

for the high frequency region peak (800–1400 cm^{-1}) with four Gaussian peaks and this is presented in Fig. 2. Tallant and Nelson[34] analysed the Raman spectrum for sodium aluminophosphate glasses and attributed the peaks observed at 1161 and 1206 cm^{-1} to the Q^2 tetrahedral units associated with sodium and the Q^2 tetrahedral units associated with alumina tetrahedral units, respectively.[35] Therefore, the bands observed at 1161 and 1213 cm^{-1} in the spectrum of NCAP glass were assigned to the Q^2 units associated with sodium and alumina, respectively. The peaks observed at 1037 cm^{-1} may possibly be assigned to the $AlPO_4$ groups in which AlO_4^- units were charge compensated by Na^+ ions. In general, in $AlPO_4$, an excess negative charge on AlO_4^- units was compensated for by the excess positive charge on the PO_4 units.

The deconvolution analysis of NCABP and NCAGP glasses for the related peak observed at the higher frequency region clearly illustrate that structural changes have occurred with the substitution of B^{3+} and Ga^{3+} for the P^{5+} cation in the NCAP glass structure. The peak appears at 1041 cm^{-1} for NCAP glass and at 1047 cm^{-1} for NCABP glass. This indicates that the bond lengths and bond angles linked with Al–O–P bonds in the $AlPO_4$ network structure were slightly rearranged with the addition of boron.[36] Furthermore, the presence of an additional peak at 985 cm^{-1} clearly showed that additional new structural units were formed within the NCABP glass. Anastasopoulou *et al.*[37] assigned the peak appearing at 985 cm^{-1} to the phosphate units connected to trigonal and tetragonal borate units. Therefore, the peak at 980 cm^{-1} in NCABP glass was assigned to the borophosphate structural units. Furthermore, it is worth noting that the intensity of the peak at 1037 cm^{-1}, which corresponded to $AlPO_4$ groups in which AlO_4^- units were charge compensated by Na^+ ions, was decreased significantly.

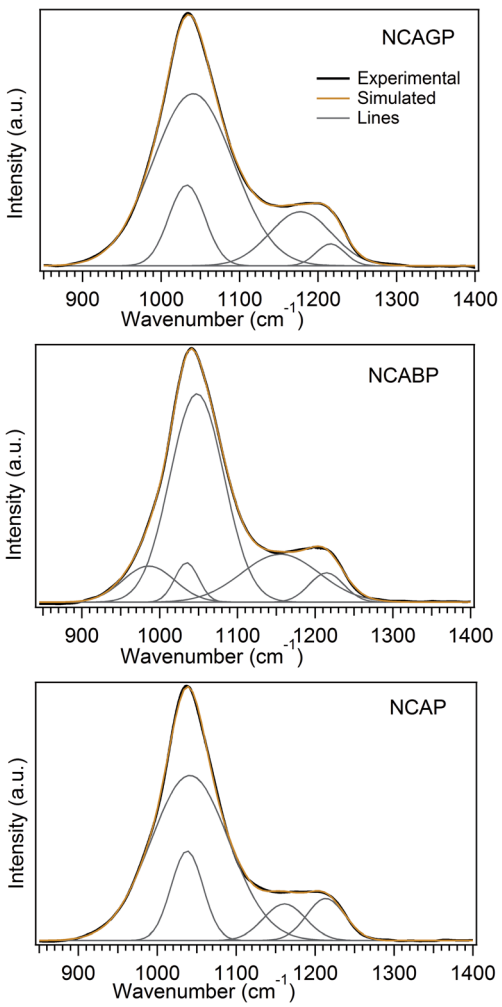

Fig. 2 Deconvolution of Raman spectra in higher wavenumber (800–1400 cm^{-1}) region.

With the Ga substitution, the concentration of Q^2 structural units associated with alumina decreased at the expense of Q^2 structural units associated with sodium. In addition, the position of the peak observed at 1161 cm^{-1} for NCAP glass was also shifted towards the higher frequency and positioned at 1177 cm^{-1} for NCAGP glass. These changes resulted from the modifications in the environment of Q^2 structural units and were directly related to the decrease in sodium concentration. Therefore, the band observed at 1177 cm^{-1} for NCAGP glass can be assigned to the Q^2 units associated with Na as well as Ga, which might be in the form of GaO_6 modifier cations.[38,39] The decrease in the Raman shift of P-non-bridging (or terminal) stretching vibrational modes with the increase in Na content in the system of Na_2O–Ga_2O_3–P_2O_5 diphosphate glasses was also attributed to the influence of the NaO_6 substitution for the GaO_6 units.[39] The variation in the intensity of the peak at 310 cm^{-1} in NCAGP glass, which can be assigned to the bending vibrations of the PO_4 units with a cation as the modifiers,[40] also confirmed the changes in the Na environment.

Considering the vibrations in the middle frequency region, the bands observed in the low frequency region at 620 cm^{-1} and 500 cm^{-1} for NCAP glass were attributed to the stretching vibrations of the AlO_5 and AlO_6 units, respectively.[38] With the substitution of boron, the intensity of the peak corresponding to the AlO_5 units had decreased and the same was observed for the AlO_6 units. These changes were possibly observed because of the rearrangements of the $AlPO_4$ network structure. However, with the substitution of Ga, the intensity of the peak corresponding to the AlO_5 units was increased significantly. Whereas, no significant changes were observed in the peak corresponding to the AlO_6 units. The bands observed at 575 and 460 cm^{-1} were assigned to the different bending vibrational modes of the network units.[37]

3.2 MAS-NMR

Fig. 3 shows the ^{27}Al MAS-NMR spectra for all the glasses. Each spectrum shows three resonance peaks including the peak at the higher chemical shift side that can be assigned to the AlO_4 units. The lowest peak can be assigned to the AlO_6 units, and the peak in the middle can be assigned to the AlO_5 units.[41] These three peaks were distinct and isolated from each other for NCAP and for NCABP glass compositions. However, the peaks corresponding to AlO_4 and AlO_5 units were overlapped with each other for the NCAGP glasses. From the multiple quantum MAS (MQMAS) spectra shown in Fig. S1 and S2 (ESI†), it was

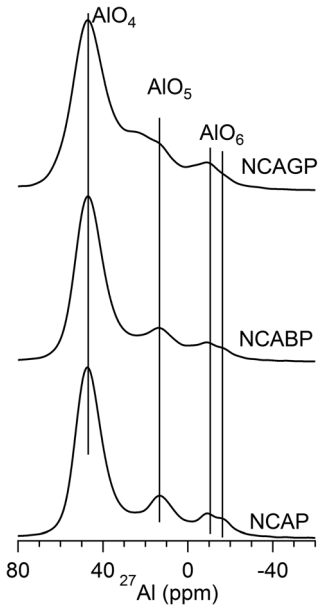

Fig. 3 ^{27}Al MAS-NMR spectra.

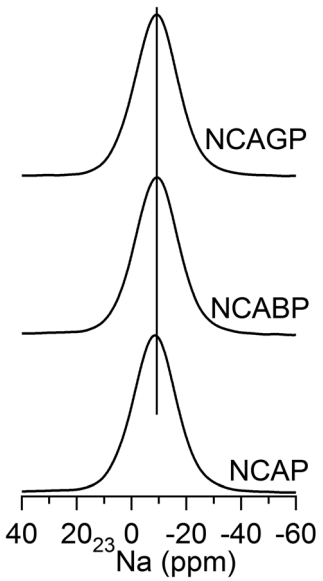

Fig. 5 ^{23}Na MAS-NMR spectra.

also clear that the AlO_4 is clearly resolved into two regions and the AlO_6 was also resolved into two regions. Furthermore, the peak typical of AlO_6 units splits into two peaks for all the glasses. Irrespective of the chemical composition and based on the quantitative analysis interpretation, all the glasses were enriched with AlO_4 units.

Fig. 4 shows the ^{31}P MAS-NMR spectra of the glasses studied. The ^{31}P MAS-NMR spectrum for NCAP glass shows two broad peaks, positioned at ~−12 ppm and ~−19 ppm, together with two shoulders: one at the higher chemical shift side (−4 ppm) and the other at the lower chemical shift side (−27 ppm). The resolution of two broad peaks decreased with the increase in the substituted cationic radius for P^{5+} cations and appeared as a single peak for high cationic radius (Ga^{3+}) substitution. However, the spectrum for each glass can be easily deconvoluted into a sum of four/five Gaussian peaks, as shown in Fig. 5. Deconvoluted results are summarised in Table 2. It was clearly observed that the chemical shift values after the deconvolution were more analogous to the values obtained for $AlPO_4$ glass and crystalline materials,[42–44] which was in accordance with the Raman experimental results. On the basis of the peak assignments for $AlPO_4$ glass- and crystalline-based materials,[42–44] it was suggested that the deconvoluted components obtained can be easily assigned to Q^0 species linked to different numbers of aluminium (Al) neighbours. In general, the building units in the aluminophosphate glass network were identified using the Q^n (mAl) nomenclature.[41,45] The index "n" is the number of phosphorus atoms and "m" is the number of aluminum atoms that are connected to the central phosphorus atom. This notation makes no distinction between AlO_4 and AlO_6 NNN atoms. Therefore, the deconvoluted curves were assigned to the various Q^0 (mAl) species (where the value of m varies from 0 to 4) as follows: the signals with the centre of peaks at around 4–7 ppm and −2 to −3 ppm could be assigned to the isolated phosphate tetrahedral associated with one and two Al atoms (*i.e.*, Q^0 (1Al) and Q^0 (2Al) species), respectively, the signals around −12 to −10 ppm and ~−19 ppm, could be attributed to Q^0 (3Al) species and Q^2 (0Al) species, respectively, and finally, the signal around −24 to −27 ppm could be assigned to Q^0 (4Al) species.[44,46,47] Table 2 clearly reveals that the majority of the signals were arising mainly because of the Q^0 (3Al) species and the Q^0 (2Al) species, indicating the higher concentration of Q^0 (3Al) species followed by Q^0 (2Al) species in all the glasses under study.

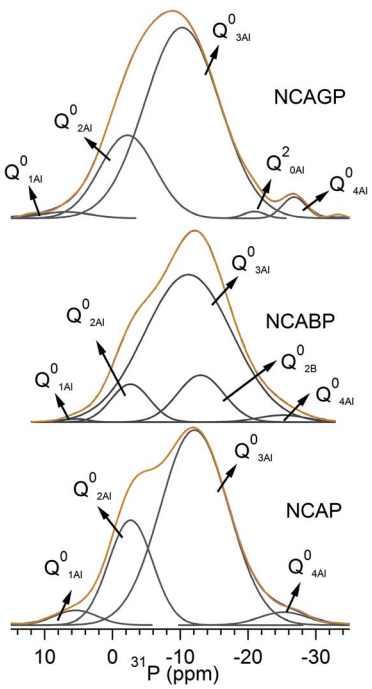

Fig. 4 ^{31}P MAS-NMR spectra. (Blue color represents the experimental spectrum, orange color represents simulated spectrum and black color represents deconvolution curves).

Table 2 ^{31}P MAS-NMR deconvolution results

	NCAP			NCABP			NCAGP		
	Peak (ppm)	Area (%)	FWHM (ppm)	Peak (ppm)	Area (%)	FWHM (ppm)	Peak (ppm)	Area (%)	FWHM (ppm)
Q^0 (1Al)	5.3	4	8.4	5.3	1	4.3	4.5	3	8
Q^0 (2Al)	−2.7	24	7.6	−2.6	8	6.6	−2.3	21	9
Q^0 (3Al)	−12.1	68	11.6	−11.2	76	15.1	−10	71	12.7
Q^0 (2B)	—	—	—	−12.9	13	8.0	—	—	—
Q^2 (0Al)	—	—	—	—	—	—	−19.3	3	8
Q^0 (4Al)	−24.8	4	9.9	−25.0	2	8.4	−26.9	2	3.8

The changes in fractions of Q^0 (*m*Al) species upon the substitution of X^{3+} cations were non-monotonic and depended on the type of X^{3+} cation in the NCAP glass composition. A significant influence of the X^{3+} cation radius was observed with the change in chemical shift values, however, systematic changes were observed only for high concentrated Q^0 (3Al) species: chemical shift values shifted towards more positive ppm values as the substituted cationic radius for P^{5+} cation increased. Because of the substitution of B^{3+} cations for P^{5+} cations, the chemical shift values of Q^0 (1Al), Q^0 (2Al) and Q^0 (3Al) were shifted towards the de-shield region (positive shift), whereas chemical shift values of Q^0 (4Al) shifted towards the shielded region (negative shift). An additional deconvoluted peak at −12.9 ppm was observed in NCABP glass. Raguenet *et al.*,[48] have assigned the peak observed at −11.7 ppm for borophosphate glasses to Q^0 (2B) structural units.[48,49] Therefore, the peak observed at −12.9 ppm for NCABP glass can be assigned to the isolated phosphorus tetrahedral units linked to boron tetrahedral units, *i.e.*, Q^0 (2B) structural units. These results suggest that the substituted B^{3+} cations show their overall effect on Q^0 (2Al) units and decrease their overall concentration at the expense of both Q^0 (3Al) and Q^0 (2B) units.

With the substitution of Ga^{3+} cations for P^{5+} cations, an additional well-resolved peak was observed at −19.3 ppm. This peak was readily attributed to Q^2 units interlinked with Na. The relative fraction of Q^0 (3Al) was increased. It is interesting to note that the chemical shift value of the Q^0 (3Al) species decreased significantly from −12.1 ppm to −10 ppm. This result indicated that some of the AlO_4 units, which were linked to Q^0 units, might be replaced with GaO_4 units. While, the chemical shift values corresponding to Q^0 (4Al) species shifted towards more negative ppm values.

^{23}Na MAS-NMR spectra of all the glasses are shown in Fig. 5. The spectra for NCAP glass displays broad resonance with the peak centre at −9 ppm. The chemical shift was slightly shifted towards lower ppm values with the substitution of B^{3+} and Ga^{3+} cations for P^{5+} cations in NCAP glass.

The ^{11}B MAS-NMR spectrum for NCABP glass is presented in Fig. 6a. The spectrum shows two broad resonance peaks placed at 15.8 ppm and 3.2 ppm. The peak at 15.8 ppm dominates the spectrum and this can be attributed to boron species in three-fold coordination (BO_3 units).[50,51] Whereas, the peak at 3.2 ppm can be attributed to boron species in four-fold coordination (BO_4 units).[50,51] The relative proportion of BO_3 units and BO_4 units, obtained from spectral integration, further revealed that 78% of the boron is placed in three-fold coordination and 22% of the boron is placed in four-fold coordination. Closer observation of the asymmetric nature towards the lower chemical shift values of the peak at 15.8 ppm clearly indicated the presence of two distinct BO_3 units [BO_3 (ring) and BO_3 (non-ring)] in the NCABP glass structure.[52] Nevertheless, the presence of a peak intensity at 15.8 ppm mainly indicated the presence of a high concentration of BO_3 (ring) type units, which are typically found in borate networks.

Fig. 6b shows the ^{71}Ga MAS-NMR spectrum for NCAGP glass. The spectrum is very broad, which is a salient feature because of very strong quadrupolar coupling of the ^{71}Ga nuclei, and is more similar to the spectra reported for the $NaPO_3$–Ga_2O_3 glasses.[53] It has been reported that the ^{71}Ga MAS-NMR spectrum is more analogous to the ^{27}Al MAS-NMR spectrum for glass materials.[54] Therefore, the three distinct signals at −38 ppm, 44 ppm and 94 ppm were attributed to GaO_6, GaO_5, and GaO_4

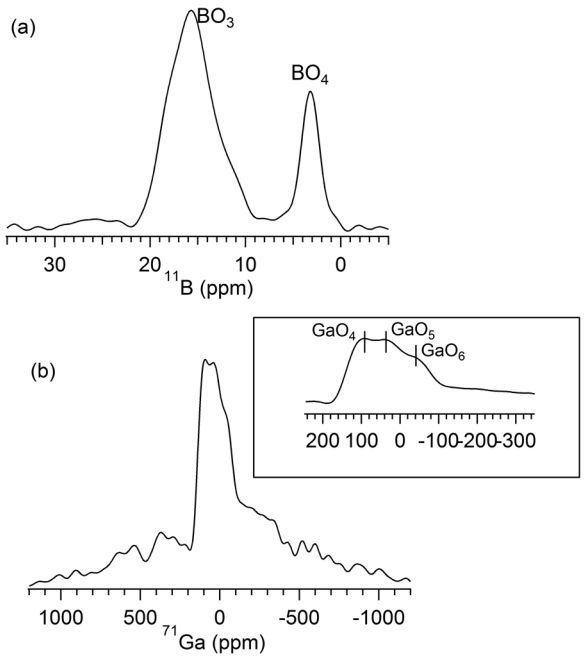

Fig. 6 (a) ^{11}B MAS-NMR spectrum for NCABP glass; and (b) ^{71}Ga MAS-NMR spectrum for NCAGP glass. Inset of (b) presents the indication of GaO_4, GaO_5 and GaO_6 chemical shifts.

units, respectively, based on the compound network.[53] The calculation of the relative proportion of these units was very difficult because of the strong anisotropic quadrupolar broadening.

3.3 Impedance analysis

Fig. 7 shows Nyquist plots for all three glass samples at 100 °C. The plots are fitted to an equivalent circuit as shown in the inset of Fig. 7. A reasonably good fit of the plots revealed a single semi-circle nature, and confirmed that there was a uniform charge transfer process in the prepared glass samples. The frequency response of the impedance of the glass samples fitted to the equivalent circuit is also shown in the inset of Fig. 7. The corresponding fitted values are listed in Table S1 (ESI†). It can be clearly seen that the diameter of the semi-circle increased when Ga and B were substituted for 'P' in the NCAP glass indicating the enhanced bulk resistance of the glass. The nature and behaviour of the impedance spectra for the Ga and B substituted glasses were similar at temperatures up to 200 °C in the present case. For all the glasses, the semi-circular nature of the impedance spectra were observed at the operating temperature of 100 °C and above indicating the free mobility of the intact Na^+ ions even at lower frequencies in the glass network. The inclined straight line at the lower frequency region was because of the electrode polarization.[55] The bulk resistance R, which is equal to Z' when $Z'' = 0$ at the lower frequency region, was used to calculate the dc conductivity, σ_{dc} of the samples using the relationship $\sigma_{dc} = [t/(R \times A)]$, where t = the thickness of the sample, and A is the applied electrode cross sectional area. At 100 °C, the dc conductivity values of NCAP, NCAGP, and NCABP were found to be 3.13×10^{-8} S cm^{-1}, 2.27×10^{-8} S cm^{-1} and 1.46×10^{-8} S cm^{-1}, respectively. The dc conductivity is a temperature dependent factor and the variation of conductivity was found to obey the well-known Arrhenius behaviour representing a straight line plot for $\ln \sigma_{dc}$ *versus* $1/T$ (where T is temperature) and the slope value of the plot can be used to determine the activation energy E_a for mobile Na^+ ions. The activation energy E_a was found to be 65.39 kJ mol^{-1}, 66.79 kJ mol^{-1} and 71.09 kJ mol^{-1} for NCAP, NCAGP, and NCABP glasses, respectively. Fig. 8 shows the dc conductivity and activation energy behaviour for Ga and B substituted NCAP glasses. The observed activation energy values were in the range similar to the other Na^+ ion conducting glasses reported in the literature.[19]

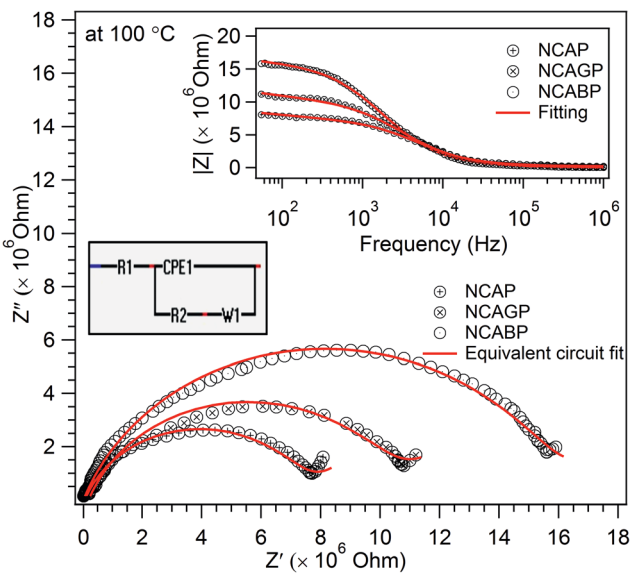

Fig. 7 The impedance spectra of the NCAP, NCABP and NCAGP glass samples at 100 °C. (Inset figures shows equivalent circuit (left side) and frequency *vs.* impedance behavior (right side)).

4. Discussion

The Raman and MAS-NMR results clearly illustrate the presence of isolated phosphorus tetrahedral units surrounded by alumina tetrahedral units as NNN in the NCAP glass structure. More precisely, the NCAP glass structure can be illustrated with the high concentration of Q^0 (3Al) units (68%) followed by Q^0 (2Al) units (24%). It has been reported that the addition of alumina into the sodium phosphate glasses directly influences the P–O–P crosslinks by replacing the P–O–P bonds with P–O–Al bonds and the network structure disrupts because of the following disproportion reaction: Q^2 (0Al) → Q^1 (mAl) → Q^0 (mAl).[41,45,46] Therefore, the presence of Q^2 (0Al) type structural units in the NCAP glass structure cannot be neglected. Despite the confirmation of Q^2 units from the high-frequency region of the Raman spectrum (as shown in Fig. 2), the indication of chemical shift values corresponding to Q^2 units was not identified from the ^{31}P MAS-NMR spectrum. This could be because of the overlap of a similar range of resonance frequencies (−20 to −25 ppm) for Q^0 (4Al) and Q^2 units.[41]

Noting that the Na–O–Al bonds or non-bridging oxygens (NBOs) for Al tetrahedra do not exist, the AlO_4 species bounded by isolated PO_4 units should not be considered as anionic. In general, the stability of the structural units can be understood based on the total bond strength, expressed in terms of valence units (VU = charge/coordination number), of the oxygen associated with the structural unit. Each alumina cation in its four-fold coordination contribute 0.75 VU to the next nearest oxygen, whereas the phosphorus ion in its isolated tetrahedral form contributes 1.25 VU to the next nearest oxygen, resulting in perfectly charge-balanced oxygen atoms within the P(4)–O–Al(4) bridges. This suggests that AlO_4 units surrounded by Q^0 units may not require charge compensation from Na^+ cations. Here that some of the modifier cations are required for compensating the charge of AlO_6 units, which are part of the Q^0 (3Al) units.[56] Nevertheless, the concentration of the AlO_6 units (~7.5%) obtained (Table 3), which are not in the proportion required for Q^0 (3Al) units, which requires 19% of AlO_6, however, from the ^{27}Al MAS-NMR spectra it was revealed that Q^0 (3Al) units were fully surrounded by AlO_4 units. It is worth mentioning that the existing AlO_6 units which are fully associated with Q^2 type tetrahedral units as proposed by Brow *et al.*,[41] may not require an additional charge compensator. Because phosphorus in Q^2 type tetrahedral contributes 1 VU to each bridging oxygen (BO) and 1.5 VU to each NBO and the required 0.5 VU can be directly

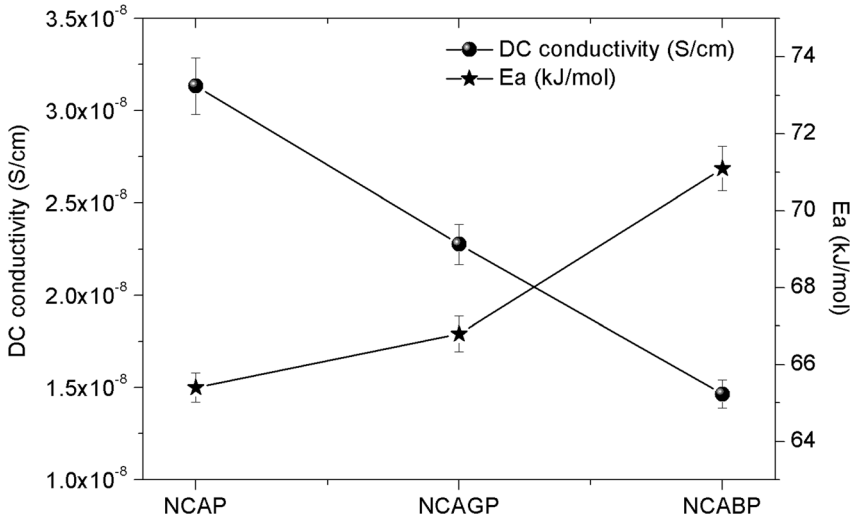

Fig. 8 Variation of dc conductivity and activation energy behaviour with the addition of gallium and boron in NCAP glass.

provided by the AlO_6 units. Overall, the MAS-NMR and Raman spectra suggest that the NCAP glass structure is more analogous to the structure of $AlPO_4$ mesoporous glass. However, the available sodium cation in NCAP glass composition disturbs the fully polymerized Q^0 (4Al) structure, which is characteristic of the $AlPO_4$ structure, into the depolymerized structure and this leaves the Q^0 (3Al) and Q^0 (2Al) units (Table 2). The changes in the chemical shift and the fraction of Q^0 (*m*Al) species (Table 2) clearly indicates the significant influence of B^{3+} and Ga^{3+} cations on the further rearrangement of the NCAP glass structure. The discussion in the next section explains the influence of Ga and B on the structure of NCAP glass and the consequence in achieving high electrical conductivity, a critical requirement for electrolyte materials.

4.1 Influence of gallium

Quantitative analysis of Q^0 (*m*Al) units requires Q^0 (2Al) and Q^0 (3Al) units to be slightly depolymerized with the addition of Ga. It has been found that both Ga and Al in oxide-based glasses often behave as network intermediates.[54] It was observed in crystalline phosphates that the ^{31}P chemical shift increases by $\approx$4 ppm for each replacement of Al^{3+} by Ga^{3+} cations because of the decrease in the P–O–Al bond angle with the substitution of Al by Ga.[57] Likewise, the ^{31}P MAS-NMR chemical shift increases on an average of 1 ppm for 5% substation of Ga for Al in $AlPO_4$ glass systems.[58] Therefore, the decrease in chemical shift of Q^0 (3Al) species illustrates that one Al site is substituted by a Ga site. The changes in the Raman spectrum for NCAGP glass suggests that some of the Na^+ cations are also replaced with Ga. Nelson and Exarhos have explained the variation in the symmetric stretch Raman frequency of the $P–O^-$ bonds with respect to the interaction between metal cation and NBO and postulated the following: increasing the O–P–O (intra tetrahedral angle) bond angle, which decreases with decrease in cation radius, decreases the stretching vibrations of the PO_2 tetrahedral.[59] In the present study, the shift in frequency of the Q^2 units, which are connected with octahedral sodium, towards a higher frequency confirms the substitution of Ga for Na. The chemical shift corresponding to the Q^2 (GaO_6) units should appear at around -7 ppm in the ^{31}P MAS-NMR spectrum.[60] Because of the overlap of this chemical shift range with the broad chemical shift range of the Q^0 (3Al) units, the presence of the Q^2 (GaO_6) units were not identified from the analysis of the ^{31}PMAS-NMR spectra. Nevertheless, the increase in full width at half maximum (FWHM) of the peak corresponding to the Q^0 (3Al) units from 11.6 ppm to 12.7 ppm confirms the contribution of the Q^2 (GaO_6) units in the total concentration of the Q^0

Table 3 Deconvolution results of ^{27}Al MAS-NMR spectra for NCAP, NCABP and NCAGP glasses

Glass	$Al(OAl)_4$	$Al(OP)_4$	$Al(OP)_5$	$Al(OAl)_6$	$Al(OP)_6$	Parameters
NCAP	60	50	26	16	−2.5	Position (ppm)
	11 549	4200	7083.09	7600	7600	CQ (quad)
	20	56	8	8	8	Integrated area (%)
NCABP	60	50	25	16	−3	Position (ppm)
	11 500	4200	7000	7600	7000	CQ (quad)
	17	62	9	6	6	Integrated area (%)
NCAGP	61	51	29	17	−1	Position (ppm)
	11 570	5000	6974	8468	6518	CQ (quad)
	19	54	12	10	5	Integrated area (%)

(3Al) units. However, it has been observed that increasing the concentration of Ga increases the Q^0 (3Ga) units in the $NaPO_3$ glass system.[53] This clearly demonstrates that the added Ga^{3+} cations in the NCAP glass system behave like Al^{3+} cations and might lead to the increase in the concentration of the Q^0 (3Al) units in the NCAGP glass system.

Deconvolution analysis of the ^{27}Al MAS-NMR spectra [Fig. S1 and S2 (ESI†)] reveals the presence of five different sites of alumina in the NCAP and NCAGP glass structure. Results obtained after the deconvolution are presented in Table 3. In general, the ^{27}Al MAS-NMR chemical shift of AlO_4 tetrahedra units depends highly on the neighbouring atom in the second coordination sphere. The ^{27}Al MAS-NMR chemical shift for the AlO_4 units moves towards zero ppm with increasing electronegativity of the neighbouring tetrahedral. Therefore, the ^{27}Al MAS-NMR chemical shift appears at around 50 ppm for the $Al(OP)_4$ units, at around 60 ppm for $Al(OSi)_4$ and at around 80 ppm for $Al(OAl)_4$ units.[61,62] Nevertheless, interesting behaviour was observed in the presence of the AlO_6 octahedron in the second coordination sphere of the AlO_4 tetrahedron: the chemical shift moves towards the shielded region and appeared at around 60 ppm. This unusual increase in chemical shift compared to that of $Al(OAl)_4$ is attributed to the increase in average Al–O bond length and an increase in coordination of the shared oxygen (four) between the AlO_4 and AlO_6 units.[61] On the contrary, it was observed that substitution of AlO_4 for PO_4 in the second coordination sphere of AlO_6 moves the chemical shift towards the deshielded region because of the low electronegativity of AlO_4.[61,62] In agreement with this, the ^{27}Al MAS-NMR chemical shifts appearing in the range of 1–12 ppm may generally be assigned to the $Al(OAl)_6$ units. The presence of deconvolution peaks at around 60 ppm and 15 ppm in the ^{27}Al MAS-NMR spectrum for NCAP glass reveals that the NCAP glass consists of an AlO_4 tetrahedron surrounded by the AlO_6 octahedron units. Therefore, the peaks appeared after the deconvolution are assigned to the following structural units: the peak at around 60 ppm is attributed to the AlO_4 tetrahedra connected to the AlO_6 octahedra units, the peak at around 50 ppm is assigned to $Al(OP)_4$ units, the peak at around 26 ppm is assigned to $Al(OP)_5$ units, the peak at around 16 ppm is allocated to $Al(OAl)_6$ units, and the peak at around −2.5 ppm is attributed to $Al(OP)_6$ units.[61] Nevertheless, the deconvolution peaks obtained from the ^{27}Al MAS-NMR spectra for NCAGP glass appeared in the more deshielded region compared to that of NCAP glass. This shift was attributed to the effect of partial substitution of Ga for Al in AlO_6 sites, which are attached to the AlO_4 tetrahedron, and Ga for P in PO_4 units, which were connected in $Al(OP)_5$ and $Al(OP)_6$ units.

The ^{27}Al MAS-NMR spectra for NCAGP glass indicates that the addition of Ga^{3+} also increased the fraction of AlO_5/AlO_6 units (Table 3). The similar increasing tendency of AlO_5/AlO_6 concentration was also observed with the increase in the concentration of Ga in the $AlPO_4$ glass structure.[58] Hee *et al.* studied the effect of progressive addition of Ga_2O_3 on the local glass structure of $NaPO_3$, and reported that Ga attains the GaO_6, GaO_5, and GaO_4 sites only in the medium concentration range of 12–25 mol% Ga_2O_3, which is much higher than the concentration in the present study.[60] The ^{71}Ga MAS-NMR spectra for NCAGP glass, which contains 6 mol% of Ga_2O_3, clearly reveals that GaO_4, GaO_5 and GaO_6 structural units are present in the NCAGP glass structure. This indicates that the Ga added competes well with the alumina intermediate cations, which generally occupy all possible polyhedral sites in the glass network structure, and might lead to the generation of a mixed-intermediate effect in the NCAGP glass system. Further experimental studies are required to examine the mixed-intermediate effect.

4.2 Influence of boron

Because of the ability of boron atoms to form BO_4 and BO_3 (ref. 49 and 52) units, the influence of the addition of boron on the NCAP structure should be dissimilar compared to that of the Ga addition. It has been stated that if boron is substituted for aluminium as a second neighbour of phosphorus, the ^{31}P chemical shift must change to be more negative.[50] The observed chemical shift at −12.9 ppm, indicative of the Q^0 (2B) units, might have occurred because of the substitution of boron for aluminium in the Q^0 (2Al) structural units, which are significantly decreased compared to that of NCAP glass. Nevertheless, the chemical shift (3.2 ppm) for the BO_4 units clearly shows that the BO_4 sites are surrounded by fewer phosphate tetrahedral units.[48,51] It can be clearly understood that because of the larger tendency of the Al^{3+} to occupy the next nearest sites of P^{5+} compared to that of B^{3+}, at high concentrations of Al_2O_3 in sodium alumina borophosphate glasses, most of the boron atoms convert from the BO_4 species to the BO_3 species.[63] The available high concentration of the BO_3 units (in the form of rings), which was revealed from the ^{11}B MAS-NMR spectra, clearly illustrate that the available BO_4 units in NCABP glass are mostly connected to the BO_3 rings and most of the boron is not connected with the phosphorus. It should be noted at this point that the formation of the BO_3 rings together with the BO_4 and PO_4 units in the NCABP glass structure might lead to the formation of small domains (in nm size) of borophosphate and borate networks, which are possibly connected through the B^3–O–B^4–O–P chains. The formation of such small domains in borophosphate and borosilicate glasses are well documented.[64,65]

The same chemical shift of four-, five- and six-coordinated aluminium compared with NCAP glass further confirms that the Al–O–B linkages are absent in NCABP glasses. The increase in intensity of the Raman vibrational band corresponding to AlO_6 units at 500 cm^{-1} and the change in chemical shift of the ^{27}Al MAS-NMR spectra for the $Al(OP)_6$ units (Table 3), further suggests that the ionic character between Al and O might be decreased through the decrease of the average Al–O bond length in the $Al(OP)_6$ unit.[31,61] This indicates the rearrangement of Q^0 (3Al) and Q^0 (2Al) units with the addition of boron. This activity could be explained based on the formation of borate and borophosphate domains in NCABP glass. In general, the excess of phosphorus is primarily responsible for the formation of the $Al(OP)_5$ and $Al(OP)_6$ units in aluminophosphate glasses.[41,58] Nevertheless, the formation of borate and borophosphate

domains decreases the excess phosphorus available for the $Al(OP)_5$ and $Al(OP)_6$ units, and thus, increases the probability for the formation of the $Al(OP)_4$ units because of the larger tendency of Al^{3+} to occupy the next nearest sites of P^{5+}. Deconvolution of the ^{27}Al MAS-NMR spectra for NCABP glass also illustrates that the $Al(OP)_4$ structural units are increased with the addition of boron. It has also been reported that the addition of boron to the aluminophosphate glasses significantly influenced the coordination of Al and AlO_4 units which have been increased compared to AlO_6 units.[66,67] This is agrees with the ^{27}Al MAS-NMR results observed for NCABP glass, where the concentration of AlO_4 units increases with the addition of boron (Table 3). This might be responsible for increasing the concentration of Q^0 (3Al) units in NCABP glass.

4.3 Ion conductivity

On the basis of the previous analysis, the structural changes associated with the Na^+ ionic conductivities in the NCAP glass can be correlated. In general, all the phosphorus Q^0 (*m*Al) species present in the network structure should be electrically neutral to neutralize the total glass. Therefore, the charges located on each species can be calculated on the basis of band valence consideration, and this is more analogous to the models proposed by Ren and Eckert[53] for alumina phosphate glasses. Considering the $AlPO_4$ structure, which contains an equal number of the AlO_4 and PO_4 units, the four oxygen atoms linking the Q^0 type phosphate unit and the Al tetrahedral unit are locally neutral by contributing 1.25 VU from phosphorus and 0.75 VU from the aluminum atom, and therefore require no additional charges. Implementing a similar model to the species present in the NCAP glass structure, Q^0 (3Al), Q^0 (2Al), Q^0 (1Al) and Q^0 (0Al) structural units require an additional charge of 0.75, 1.5, 2.25 and 3 VU, respectively. In the present case, highly mobile Na^+ provide the required additional charges for the Q^0 (*m*Al) units. Nevertheless, the high concentration of the Q^0 (3Al) units requires a smaller number of sodium cations (0.75 VU for each Q^0 (3Al) unit). The continuous network structure of the Q^0 (3Al) units leads to supression of the hopping sites required for long-range motion of the mobile sodium ions. In addition, the existence of several environments for alumina, as is revealed from the broad signals of ^{27}Al MAS-NMR spectra, also suggests the discontinuity of the electric field limiting conduction process in the NCAP glass structure. These results support the fact that lower mobile ion conductivity was achieved from NCAP glass that from any other types of NASICON glasses.[68]

The changes in the environment of the Na^+ cation in the NCABP and NCAGP glasses are also accounted for from the observation of changes in ^{23}Na MAS-NMR spectra. In general, the ^{23}Na MAS-NMR chemical shift is highly sensitive to the coordination number and the Na–O bond length. The ^{23}Na chemical shift is correlated well with the Na–O bond length because the chemical shift decreases with the increasing average bond length. Apparently, the increase in coordination number leads to an increase in the Na–O bond length and thereby increasing the interaction.[69] Therefore, the decrease in the ^{23}Na chemical shift value clearly suggests a strong interaction of Na^+ cations with the Q^0 (*m*Al) species in boron and Ga containing glasses, than in the NCAP glass. In support of this, the experimental conductivity results revealed that the electrical conductivity was decreased with the addition of Ga and was decreased even further with the addition of boron. The significant decrease in the conductivity of NCABP glass could be because of the formation of borate and borophosphate domains.[50] The conductivity of NCAGP glass was slightly decreased because of the possible mixed intermediate effect. In addition, the formation of a high concentration of AlO_5/AlO_6 units, which generally compensates the charge of the Q^0 (*m*Al) units instead of the Na^+ cation, when compared to that of NCAP glasses also increases the distance between the hopping centres for Na^+ ion mobility.[68] The previous results suggest that decreasing the Q^0 (3Al) units and increasing the charge compensation centres in the network structure might increase the conductivity of the NCAP glass. Therefore, further experimental studies are required to enhance the ionic conductivity at RT for the NCAP glass to be useful for Na-ion batteries.

5. Conclusions

In summary, the structural and electrical properties of sodium super ionic conductor (NASICON) based phosphate glasses having the chemical formula $Na_{2.8}Ca_{0.1}Al_2P_3O_{12}$ (NCAP) were evaluated thoroughly using Raman, MAS-NMR, and impedance spectroscopy techniques. Furthermore, the influence of boron and gallium on the structural and electrical properties of NCAP glass were also studied. The NCAP glass network structure consists of a high concentration of the Q^0 (3Al) units followed by the Q^0 (2Al) units, as confirmed from the Raman and ^{31}P MAS-NMR spectra. A high concentration of the Q^0 (3Al) units leads to suppression of the hopping sites required for long-range motion of the mobile sodium ions, which is also responsible for the low conductivity achieved compared to the other NASICON based glasses. The ^{27}Al MAS-NMR spectra further indicate that aluminium plays a major role in constructing the NCAP structure. The existence of alumina in five different sites might impede the electric field, which further limits the mobility of the Na^+ in the NCAP glass structure. ^{11}B and ^{31}P MAS-NMR spectra for NCABP glass indicate that boron cations in the NCABP glass structure interacted with phosphorus cations and created the borate and borophosphate domains by forming B_3–O–B_4–O–P_4 linkages. Formation of domains and the increased fraction of the Q^0 (3Al) units significantly reduced the conductivity of NCABP glass compared to that of NCAP glass. Gallium competed with the aluminium cations and partially occupied the possible four, five and six coordination sites for alumina in NCAP glass, as revealed from the ^{27}Al and ^{71}Ga MAS-NMR spectrum for NCAGP glass. A slight increase in the Q^0 (3Al) units and disturbance in the arrangement of alumina occupied sites slightly reduced the conductivity of the NCAGP glass. Results obtained from the present study indicate that reducing the overall concentration of the Q^0 (3Al) units and limiting the distribution of alumina sites might improve the Na-ion conductivity in the NCAP glass.

Conflicts of interest

There are no conflicts to declare.

Acknowledgements

ARA, SB, KB and KA gratefully acknowledge the support and encouragement of Dr K. Muraleedharan, Director, CSIR-CGCRI and Dr Ranjan Sen, Head, Glass Division, CSIR-Central Glass & Ceramic Research Institute. ARA would like to thank to Prof. Gaddam Vijaya Prakash for his approval for carrying out further studies on $Na_3Al_2P_3O_{12}$ glass compositions. Useful suggestions and discussions from Dr S. Mahanty are greatly acknowledged. The use of the Bruker AV 700 MHz NMR spectrometer in the Central NMR Facility, CSIR-NCL, purchased under the Twelfth Five Year Plan Project CSC0405 is gratefully acknowledged. ARA acknowledges the support of Dr R. N. Basu, Head, Fuel Cell and Battery Division, CSIR-CGCRI for doing conductivity measurements.

References

1 Y. Sun, *Chem. Soc. Rev.*, 2017, **46**, 3529–3614.
2 J. B. Goodenough, *ACS Catal.*, 2017, **7**, 1132–1135.
3 Y. Nishi, *J. Power Sources*, 2001, **100**, 101–106.
4 J. Tang, A. D. Dysart and V. G. Pol, *Curr. Opin. Chem. Eng.*, 2015, **9**, 34–41.
5 K. Kubota and S. Komaba, *J. Electrochem. Soc.*, 2015, **162**, 2538–2550.
6 Z. Zhang, Q. Zhang, C. Ren, F. Luo, Q. Ma, Y.-S. Hu, Z. Zhou, H. Li, X. Huang and L. Chen, *J. Mater. Chem. A*, 2016, **4**, 15823–15828.
7 F. Lalere, V. Seznec, M. Courty, R. David, J. N. Chotard and C. Masquelier, *J. Mater. Chem. A*, 2015, **3**, 16198–16205.
8 L. P. Wang, L. Yu, X. Wang, M. Srinivasan and Z. J. Xu, *J. Mater. Chem. A*, 2015, **3**, 9353–9378.
9 K. Vignarooban, R. Kushagra, A. Elango, P. Badami, B.-E. Mellander, X. Xu, T. G. Tucker, C. Nam and A. M. Kannan, *Int. J. Hydrogen Energy*, 2016, **41**, 2829–2846.
10 W. Zhou, Y. Li, S. Xin and J. B. Goodenough, *ACS Cent. Sci.*, 2017, **3**, 52–57.
11 J.-J. Kim, K. Yoon, I. Park and K. Kang, *Small Methods*, 2017, **1**, 1700219.
12 I.-H. Chu, C. S. Kompella, H. Nguyen, Z. Zhu, S. Hy, Z. Deng, Y. S. Meng and S. P. Ong, *Sci. Rep.*, 2016, **6**, 33733.
13 Y. S. Zhu, L. L. Li, C. Y. Li, L. Zhou and Y. P. Wu, *Solid State Ionics*, 2016, **289**, 113–117.
14 S. Song, H. M. Duong, A. M. Korsunsky, N. Hu and L. Lu, *Sci. Rep.*, 2016, **6**, 32330.
15 S. K. Kim, A. Mao, S. Sen and S. Kim, *Chem. Mater.*, 2014, **26**, 5695–5699.
16 Y. Ni, R. Zheng, X. Tan, W. Yue, P. Lv, J. Yang, D. Song, K. Yu and W. Wei, *J. Mater. Chem. A*, 2015, **3**, 17558–17562.
17 D. E. Watson and S. W. Martin, *J. Non-Cryst. Solids*, 2017, **471**, 39–50.
18 R. Christensen, G. Olson and S. W. Martin, *J. Phys. Chem. B*, 2013, **117**, 16577–16586.
19 L. Moreno-Real, P. Maldonado-Manso, L. Leon-Reina, E. R. Losilla, F. E. Mouahid, M. Zahir and J. Sanz, *J. Mater. Chem.*, 2002, **12**, 3681–3687.
20 H.-P. Hong, *Mater. Res. Bull.*, 1976, **11**, 173–182.
21 J. B. Goodenough, H.-P. Hong and J. A. Kafalas, *Mater. Res. Bull.*, 1976, **11**, 203–220.
22 I. Lisenker and C. R. Stoldt, *Front. Energy Res.*, 2016, **4**, 13.
23 A. A. Reddy, U. Tulyaganov, V. V Kharton and J. M. F. Ferreira, *J. Solid State Chem.*, 2015, **19**, 2899–2916.
24 K. Kanehori, K. Matsumoto, K. Miyauchi and T. Kudo, *Solid State Ionics*, 1983, **9–10**, 1445–1448.
25 S. Li, J. Cai and Z. Lin, *Solid State Ionics*, 1988, **28–30**, 1265–1270.
26 B. E. Francisco, C. R. Stoldt and J.-C. M'Peko, *J. Phys. Chem. C*, 2015, **119**, 16432–16442.
27 M. de Oliveira, T. S. Gonçalves, C. Ferrari, C. J. Magon, P. S. Pizani, A. S. S. de Camargo and H. Eckert, *J. Phys. Chem. C*, 2017, **121**, 2968–2986.
28 I. R. Evans, J. S. O. Evans, H. G. Davies, A. R. Haworth and M. L. Tate, *Chem. Mater.*, 2014, **26**, 5187–5189.
29 E. R. Losilla, M. A. G. Aranda, M. A. Paris and A. R. West, *Chem. Mater.*, 1998, **10**, 665–673.
30 A. A. Reddy, D. U. Tulyaganov, G. C. Mather, S. Rodr, S. Das, M. J. Pascual, F. Mun, J. Senker and J. M. F. Ferreira, *J. Phys. Chem. C*, 2015, **119**, 11482–11492.
31 A. R. Allu, S. Balaji, D. U. Tulyaganov, G. C. Mather, F. Margit, M. J. Pascual, R. Siegel, W. Milius, J. Senker, D. A. Agarkov, V. V Kharton and J. M. F. Ferreira, *ACS Omega*, 2017, **2**, 6233–6243.
32 D. Massiot, F. Fayon, M. Capron, I. King, S. Le Calvé, B. Alonso, J.-O. Durand, B. Bujoli, Z. Gan and G. Hoatson, *Magn. Reson. Chem.*, 2002, **40**, 70–76.
33 J. Yifen, J. Dehua, C. Xiangsheng, B. Beiya and H. Xihuai, *J. Non-Cryst. Solids*, 1986, **80**, 147–151.
34 D. R. Tallant and C. Nelson, *Phys. Chem. Glasses*, 1986, **27**, 75.
35 A. Moguš-Milanković, A. Gajović, A. Šantić and D. E. Day, *J. Non-Cryst. Solids*, 2001, **289**, 204–213.
36 G. B. Rouse, P. J. Miller and W. M. Risen, *J. Non-Cryst. Solids*, 1978, **28**, 193–207.
37 M. Anastasopoulou, K. C. Vasilopoulos, D. Anagnostopoulos, I. Koutselas, D. K. Papayannis and M. A. Karakassides, *J. Phys. Chem. B*, 2017, **121**, 4610–4619.
38 A. Belkébir, J. Rocha, A. P. Esculcas, P. Berthet, B. Gilbert, Z. Gabelica, G. Llabres, F. Wijzen and A. Rulmont, *Spectrochim. Acta, Part A*, 1999, **55**, 1323–1336.
39 A. Belkébir, J. Rocha, A. P. Esculcas, P. Berthet, B. Gilbert, Z. Gabelica, G. Llabres, F. Wijzen and A. Rulmont, *Spectrochim. Acta, Part A*, 2000, **56**, 435–446.
40 Y. M. Lai, X. F. Liang, S. Y. Yang, J. X. Wang and B. T. Zhang, *J. Mol. Struct.*, 2012, **1013**, 134–137.
41 R. K. Brow, R. J. Kirkpatrick and G. L. Turner, *J. Am. Ceram. Soc.*, 1993, **76**, 919–928.
42 Z. Zhao, S. Xu, M. Y. Hu, X. Bao and J. Z. Hu, *J. Phys. Chem. C*, 2016, **120**, 1701–1708.
43 S. Delsarte, P. Grange, T. Chen, P. Grobet and P. Jacobs, *J. Phys. Chem. B*, 2003, **107**, 6504–6510.

44 L. Zhang, A. Bögershausen and H. Eckert, *J. Am. Ceram. Soc.*, 2005, **88**, 897–902.
45 R. K. Brow, *J. Non-Cryst. Solids*, 2000, **263&264**, 1–28.
46 J. M. Egan, R. M. Wenslow and K. T. Mueller, *J. Non-Cryst. Solids*, 2000, **261**, 115–126.
47 L. Zhang and H. Eckert, *J. Mater. Chem.*, 2004, **14**, 1605–1615.
48 B. Raguenet, G. Tricot, G. Silly, M. Ribes and A. Pradel, *J. Mater. Chem.*, 2011, **21**, 17693–17704.
49 G. Tricot, K. Ben Tayeb, L. Koudelka, P. Mosner and H. Vezin, *J. Phys. Chem. C*, 2016, **120**, 9443–9452.
50 N. Mascaraque, A. Durán and F. Muñoz, *J. Non-Cryst. Solids*, 2011, **357**, 3212–3220.
51 F. Muñoz, L. Montagne, L. Pascual and A. Durán, *J. Non-Cryst. Solids*, 2009, **355**, 2571–2577.
52 K. Januchta, R. E. Youngman, A. Goel, M. Bauchy, S. L. Logunov, S. J. Rzoska, M. Bockowski, L. R. Jensen and M. M. Smedskjaer, *Chem. Mater.*, 2017, **29**, 5865–5876.
53 J. Ren and H. Eckert, *J. Phys. Chem. C*, 2014, **118**, 15386–15403.
54 S. M. Bradley, R. F. Howe and R. A. Kydd, *Magn. Reson. Chem.*, 1993, **31**, 883–886.
55 I. M. Hodge, M. D. Ingram and A. R. West, *J. Electroanal. Chem. Interfacial Electrochem.*, 1976, **74**, 125–143.
56 S. Wegner, L. Van Wu and G. Tricot, *J. Non-Cryst. Solids*, 2008, **354**, 1703–1714.
57 S. K. Kulshreshtha, O. D. Jayakumar and V. Sudarsan, *J. Phys. Chem. Solids*, 2004, **65**, 1141–1146.
58 J. He, P. Ma, G. Zhang, R. Li and L. Zhang, *RSC Adv.*, 2016, **6**, 99149–99157.
59 B. N. Nelson and G. J. Exarhos, *J. Chem. Phys.*, 1979, **71**, 2739–2747.
60 P. Hee, R. Christensen, Y. Ledemi, J. E. C. Wren, M. Dussauze, T. Cardinal, E. Fargin, S. Kroeker and Y. Messaddeq, *J. Mater. Chem. C*, 2014, **2**, 7906–7917.
61 D. Muller, W. Gessner, A. Samoson, E. Lippmaa and G. Scheler, *J. Chem. Soc., Dalton Trans.*, 1986, 1277–1281.
62 R. Hussin, D. Holland and R. Dupree, *J. Non-Cryst. Solids*, 2002, **298**, 32–42.
63 K. Januchta, R. E. Youngman, A. Goel, M. Bauchy, S. J. Rzoska, M. Bockowski and M. M. Smedskjaer, *J. Non-Cryst. Solids*, 2017, **460**, 54–65.
64 Y. Yu and M. Eden, *RSC Adv.*, 2016, **6**, 101288–101303.
65 A. Saitoh, G. Tricot, P. Rajbhandari, S. Anan and H. Takebe, *Mater. Chem. Phys.*, 2015, **149–150**, 648–656.
66 Y. Z. Khimyak and J. Klinowski, *J. Mater. Chem.*, 2002, **12**, 1079–1085.
67 L. van Wüllen, S. Wegner and G. Tricot, *J. Phys. Chem. B*, 2007, **111**, 7529–7534.
68 D. R. Clayton, D. Lepage, P. N. Plassmeyer, C. J. Page and M. C. Lonergan, *RSC Adv.*, 2017, **7**, 7046–7051.
69 A. M. George, S. Sen and J. F. Stebbins, *Solid State Nucl. Magn. Reson.*, 1997, **10**, 9–17.